Simulation of dose uniformity for different pulse durations during inner surface plasma immersion ion implantation

A. G. Liu, X. F. Wang, S. Y. Wang, B. Y. Tang, and P. K. Chu[a)]
Department of Physics and Material Science, City University of Hong Kong, 83 Tat Chee Avenue, Kowloon, Hong Kong

Z. M. Zeng and X. B. Tian
Advanced Welding and Production Technology National Key Laboratory, Harbin Institute of Technology, 92 West Da Zhi Street, Harbin 150006, China

(Received 4 June 1998; accepted 12 October 1998)

Without the line-of-sight limitation, plasma immersion ion implantation (PIII) emulates conventional beam-line ion implantation in inner surface modification of industrial components. However, dose uniformity on the inner surface is critical. Inner surface PIII of a cylindrical bore is modeled using a two-dimensional fluid model. It is found that the retained dose is not uniformly distributed on the inner surface and the maximum dose is observed away from the edge. The exact location of the maximum dose, which varies with the implant pulse duration, is closer to the center when the pulse width is longer. The maximum relative difference of the retained dose along the interior also depends on the implant pulse duration. It is smaller for a longer pulse duration after a threshold value has been exceeded. © *1999 American Vacuum Society.* [S0734-211X(99)02202-7]

I. INTRODUCTION

Plasma immersion ion implantation (PIII)[1,2] circumvents the line-of-sight restriction and is considered a proper method for inner surface modification. Sun *et al.*[3] analyzed the inner surface PIII process using a filament plasma source and found that the plasma density was lower than that on the outside and suggested the use of a coaxial auxiliary anode for improvement. Sheridan[4–6] simulated the inner surface PIII process of a bore using a one-dimensional fluid model and concluded that the impact energy was low. It was pointed out that as the plasma sheath inside the bore overlapped, the ions were not fully accelerated. They were thus implanted into the inner surface with low impact energy. Other theoretical studies[7–11] have focused on the effects of the bore radius, electrode's radius, and rise time of the pulse when an auxiliary electrode is used.

Recently, experiments have been conducted to investigate inner surface coating[12] and inner surface PIII.[13,14] The results indicate that even though the impact energy and retained dose are improved using the auxiliary electrode, the implant dose is not very uniform along the interior surface. Contrary to conventional wisdom, the highest retained dose is found to occur at a distance from the rim of the cylindrical bore.[13,14] In this article, we present a two-dimensional fluid model to explain this phenomenon and use the model to investigate the effects of the implant pulse width.

II. MODEL

The applied voltage φ_t is usually several tens of kV in PIII and the kinetic energy of ions and electrons can be neglected compared with $e|\varphi_t|$. In the typical sub-mTorr pressure range used in PIII, the average mean free path is much larger than the sheath thickness, and so the inner surface PIII process can be described by a collisionless, cold plasma fluid model. In this model, the electron density is assumed to satisfy Boltzmann's distribution, and the ion density and velocity can be described using the mass continuity equation and momentum continuity equation of a compressable fluid in a conserving form:

$$\frac{\partial n_i}{\partial t}+\nabla\cdot(n_i\mathbf{v})=0, \tag{1}$$

$$\frac{\partial}{\partial t}(n_i v)+\nabla\cdot(n_i v\mathbf{v})=-\frac{en_i}{m_i}\nabla\varphi, \tag{2}$$

where n_i is the ion density, t is the implant time, $\mathbf{v}$ is the ion velocity, e is the electron charge, m_i is the ion mass, and φ is the potential. The potential distribution can be derived using Poisson's equation:

$$\nabla^2\varphi=-\frac{e}{\varepsilon_0}(n_i-n_e), \tag{3}$$

where ε_0 is the vacuum permitivity and n_e is the electron density. To satisfy Boltzmann's distribution,

$$n_e=n_0\exp\left(\frac{e\varphi}{kT_e}\right), \tag{4}$$

where n_0 is plasma density, k is the Boltzmann constant, and T_e is the electron temperature.

a)Electronic mail: paul.chu@cityu.edu.hk

Due to the axial symmtry of the bore, the process can be simulated in a cylindrical coordinate system. The equations become

$$\frac{\partial n_i}{\partial t}+\frac{1}{r}\frac{\partial}{\partial r}(rn_iv_r)+\frac{\partial}{\partial z}(n_iv_z)=0, \tag{5}$$

$$\frac{\partial}{\partial t}(n_iv_r)+\frac{1}{r}\frac{\partial}{\partial r}(rn_iv_r^2)+\frac{\partial}{\partial z}(n_iv_rv_z)=-\frac{en_i}{m_i}\nabla\varphi_r, \tag{6}$$

$$\frac{\partial}{\partial t}(n_iv_z)+\frac{1}{r}\frac{\partial}{\partial r}(rn_iv_zv_r)+\frac{\partial}{\partial z}(n_iv_z^2)=-\frac{en_i}{m_i}\nabla\varphi_z, \tag{7}$$

$$\frac{1}{r}\frac{\partial}{\partial r}\left(r\frac{\partial\varphi}{\partial r}\right)+\frac{\partial^2\varphi}{\partial z^2}=-\frac{e}{\varepsilon_0}\left[n_i-\exp\left(\frac{e\varphi}{kT_e}\right)\right], \tag{8}$$

where r and z are the radial and axial coordinates, respectively, and v_r and v_z are the radial and axial components of the ion velocity. To normalize the equations, let

$$\rho=\frac{r}{S},\quad Z=\frac{z}{S},\quad \phi=\frac{\varphi}{\varphi_t},\quad N=\frac{n_i}{n_0},\quad V_\rho=\frac{v_r}{v_{\max}},$$

$$V_Z=\frac{v_z}{v_{\max}},\quad \text{and}\quad T=t\omega_{\rm pi},$$

where

$$S=\sqrt{\frac{-4\varepsilon_0\varphi_t}{en_0}}$$

is the overlapped sheath radius,

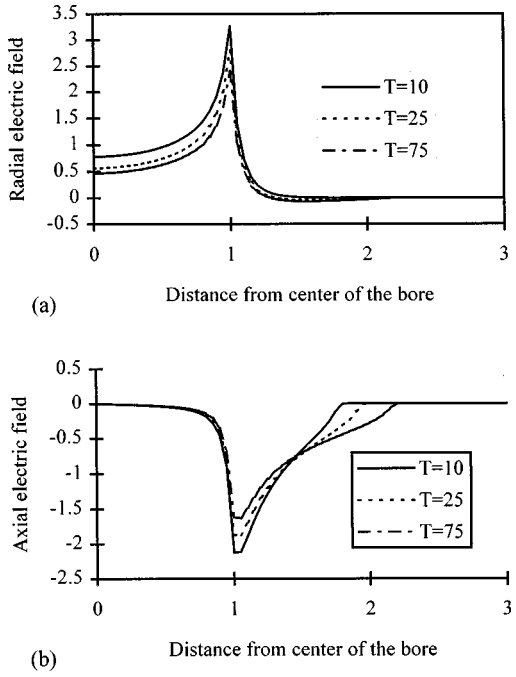

FIG. 1. Distribution of (a) radial electric field and (b) axial electric field at $R=0.95$ at different time.

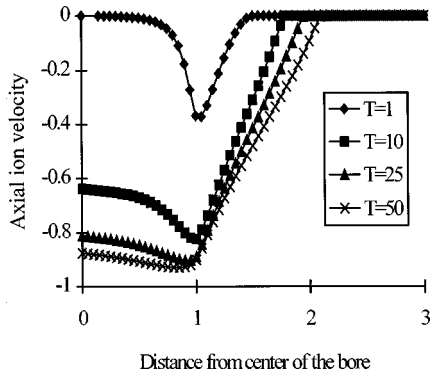

FIG. 2. Axial ion velocity distribution at $R=1.0$ at different time.

$$v_{\max}=\sqrt{\frac{-2e\varphi_t}{m_i}}$$

is the maximum ion velocity, and

$$\omega_{\rm pi}=\sqrt{\frac{n_0e^2}{\varepsilon_0m_i}}$$

is the ion frequency. When $n_i\neq 0$, Eqs. (5)–(8) become

$$\frac{\partial N}{\partial T}+\frac{1}{\sqrt{2}}\left(V_\rho\frac{\partial N}{\partial\rho}+N\frac{\partial V_\rho}{\partial\rho}+\frac{NV_\rho}{\rho}+V_Z\frac{\partial N}{\partial Z}+N\frac{\partial V_Z}{\partial Z}\right)=0, \tag{9}$$

$$\frac{\partial V_\rho}{\partial T}+\frac{1}{\sqrt{2}}V_\rho\frac{\partial V_\rho}{\partial\rho}+\frac{1}{\sqrt{2}}V_Z\frac{\partial V_\rho}{\partial Z}=\frac{1}{2\sqrt{2}}\frac{\partial\phi}{\partial\rho}, \tag{10}$$

$$\frac{\partial V_Z}{\partial T}+\frac{1}{\sqrt{2}}V_\rho\frac{\partial V_Z}{\partial\rho}+\frac{1}{\sqrt{2}}V_Z\frac{\partial V_Z}{\partial Z}=\frac{1}{2\sqrt{2}}\frac{\partial\phi}{\partial Z}, \tag{11}$$

$$\frac{1}{\rho}\frac{\partial}{\partial\rho}\left(\rho\frac{\partial\phi}{\partial\rho}\right)+\frac{\partial^2\phi}{\partial Z^2}=4\left[N-\exp\left(\frac{e\varphi_t}{kT_e}\phi\right)\right]. \tag{12}$$

Assume that $\phi_{\rm last}$ is the potential distribution at the last time step and if

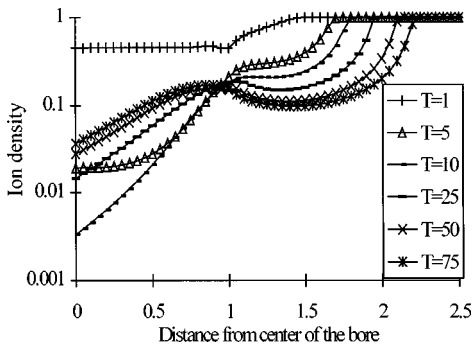

FIG. 3. Ion density distribution at $R=1.0$ of different time.

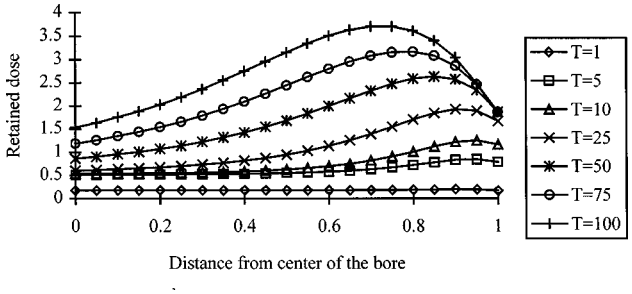

FIG. 4. Distribution of retained dose on inner surface at different time.

$$\left|\frac{e\varphi_t}{kT_e}\phi-\frac{e\varphi_t}{kT_e}\phi_{\text{last}}\right|\ll 1,$$

$$\exp\left(\frac{e\varphi_t}{kT_e}\phi\right)=\exp\left(\frac{e\varphi_t}{kT_e}\phi\right)\cdot\exp\left(\frac{e\varphi_t}{kT_e}\phi_{\text{last}}-\frac{e\varphi_t}{kT_e}\phi_{\text{last}}\right)$$

$$\approx\exp\left(\frac{e\varphi_t}{kT_e}\phi_{\text{last}}\right)\left(1+\frac{e\varphi_t}{kT_e}\phi-\frac{e\varphi_t}{kT_e}\phi_{\text{last}}\right). \quad (13)$$

Poisson's equation can be written as

$$\frac{1}{\rho}\frac{\partial}{\partial\rho}\left(\rho\frac{\partial\phi}{\partial\rho}\right)+\frac{\partial^2\phi}{\partial Z^2}$$

$$=4\left[N-\exp\left(\frac{e\varphi_t}{kT_e}\phi_{\text{last}}\right)\left(1+\frac{e\varphi_t}{kT_e}\phi-\frac{e\varphi_t}{kT_e}\phi_{\text{last}}\right)\right]. \quad (14)$$

The equations can be solved numerically using the appropriate boundary conditions to derive the ion density and velocity evolution.

The bore length is 2, bore radius is 1.5, and wall thickness is 0.1. The left boundary of the simulated region is the bore axis, and the bottom boundary is the symmetry plane of the bore. There is no right or top boundary as it is assumed that the sheath will never expand close to the vacuum chamber and their states will not affect the implant process. Hence, at the top or right boundary, the boundary conditions are $\phi|_\infty=0$, $N|_\infty=1$, $V_\rho|_\infty=0$, and $V_Z|_\infty=0$. At the left boundary, $\partial\phi/\partial\rho|_{\rho=0}=0$, $\partial N/\partial\rho|_{\rho=0}=0$, and $V_\rho|_{\rho=0}=0$, whereas at the bottom boundary, $\partial\phi/\partial Z|_{Z=0}=0$ and $\partial N/\partial Z|_{Z=0}=0$.

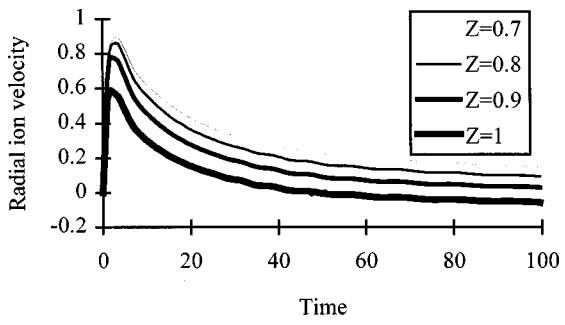

FIG. 5. Evolution of radial ion velocity on inner surface.

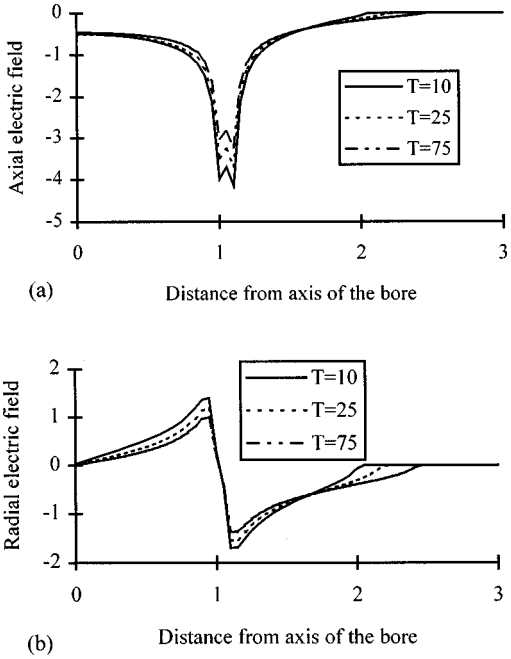

FIG. 6. Distribution of (a) axial electric field and (b) radial electric field at $Z=1.05$ at different time.

III. RESULTS AND DISCUSSION

Figure 1 displays the electric field distribution on the inner surface at $R=0.95$. It can be observed that both the radial and axial electric field components decrease with time as a result of sheath overlapping. The negative axial electric field accelerates ions towards the bore and gives rise to a negative axial velocity component. Because of the concentration of the electric field, the axial velocity evolves faster at the edge of the bore than inside the bore, as shown in Fig. 2. The ion flux penetrates inward and causes an increase in the axial velocity deep inside the bore. At $T=50$, the difference between the edge and inside is very small. The large axial velocity at the edge also causes a higher ion density at a certain distance away from the rim of the bore after some time. Figure 3 depicts the ion density distribution at different time. The ion density outside the bore diminishes with time whereas the ion density inside the bore decreases initially

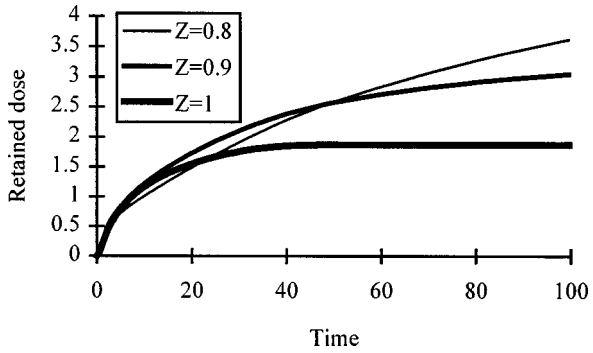

FIG. 7. Evolution of retained dose on inner surface.

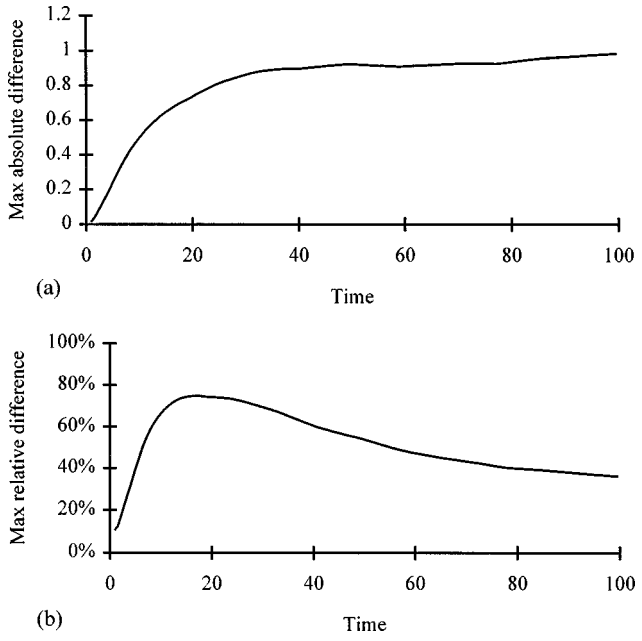

FIG. 8. Development of (a) maximum absolute difference and (b) maximum relative difference of retained dose vs time.

and then increases slightly from $T=10$ to 100. It can also be noted that after $T=25$, the peak begins to move towards the center of the bore.

The varying density results in a nonuniform dose distribution on the inner surface as exhibited in Fig. 4. However, the dose peak does not correspond exactly to the density peak. For instance, at $T=75$, the maximum dose appears at $Z=0.8$ while the maximum density is at $Z=0.9$. The dose peak thus moves faster. To explain this phenomenon, the effects of the radial ion velocity must be taken into account. Figure 5 exhibits the evolution of the radial velocity at different positions. The radial velocity is lower closer to the edge of the bore. In fact, at the edge, the radial velocity becomes negative after $T=50$. Figure 6 exhibits the electric field distribution at $Z=1.05$, that is, just outside the bore. The axial electric field shown in Fig. 6(a) accelerates ions into the bore while the radial electric field component changes the ion trajectories to achieve implantation. The positive electric field left of the bore wall accelerates ions to the right as shown in Fig. 1(a). The negative electric field accelerates ions to the left as shown in Fig. 6(a). This causes a negative radial ion velocity near the edge as illustrated in Fig. 5. The ions change direction and go towards the inner surface again by the positive radial electric field in the bore. The radial ion flux near the edge of the bore thus increases only before ions outside of the bore reach there, and after then, it begins to decrease and even changes direction. Hence, even though the ion density near the edge is high, the retained dose in this region does not increase significantly as shown in Fig. 7.

Figure 8 depicts the evolution of the maximum absolute and relative difference of the retained dose on the inner surface. The maximum absolute difference continues to increase with time, albeit very slowly after $T=30$. The maximum relative difference increases precipitously before $T=17$ similar to the absolute difference. However, after $T=17$, it begins to diminish. The maximum relative difference at $T=17$ is 74.8% and decreases to 36.1% at $T=100$. Therefore, to achieve better uniformity for inner surface PIII, a long pulse duration is preferred.

IV. CONCLUSION

Our results show that the retained dose is not uniform along the inner surface and the maximum dose is located at a distance away from the edge. The absolute location of the maximum dose depends on the implant pulse duration and moves inward as the pulse width increases. The maximum relative difference of the retained dose is also found to vary with the implant pulse duration and diminishes after exceeding a threshold pulse width.

ACKNOWLEDGMENTS

The work is supported by City University of Hong Kong Strategic Research Grant No. 7000730 and Hong Kong RGC Earmarked Grant Nos. 9040332 and 9040344.

[1]J. R. Conrad, J. Appl. Phys. **62**, 777 (1987).
[2]P. K. Chu, S. Qin, C. Chan, N. W. Cheung, and L. A. Larson, Mater. Sci. Eng., R. **17**, 207 (1996).
[3]M. Sun, S. Yang, and B. Li, J. Vac. Sci. Technol. A **14**, 367 (1996).
[4]T. E. Sheridan, J. Appl. Phys. **74**, 4903 (1993).
[5]T. E. Sheridan, Phys. Plasmas **1**, 3485 (1994).
[6]T. E. Sheridan, J. Appl. Phys. **80**, 66 (1996).
[7]X. C. Zeng, B. Y. Tang, and P. K. Chu, Appl. Phys. Lett. **69**, 3815 (1996).
[8]X. C. Zeng, T. K. Kwok, A. G. Liu, P. K. Chu, and B. Y. Tang, Appl. Phys. Lett. **71**, 1035 (1997).
[9]X. C. Zeng, A. G. Liu, T. K. Kwok, P. K. Chu, and B. Y. Tang, Phys. Plasmas **4**, 1 (1997).
[10]X. C. Zeng, T. K. Kwok, A. G. Liu, P. K. Chu, and B. Y. Tang, J. Appl. Phys. **83**, 44 (1998).
[11]T. E. Sheridan, T. K. Kwok, and P. K. Chu, Appl. Phys. Lett. **72**, 1826 (1998).
[12]S. M. Malik, R. P. Fetherston, and J. R. Conrad, J. Vac. Sci. Technol. A **15**, 2875 (1997).
[13]A. G. Liu, X. F. Wang, Q. C. Chen, B. Y. Tang, and P. K. Chu, Nucl. Instrum. Methods Phys. Res. B **143**, 306 (1998).
[14]A. G. Liu, X. F. Wang, B. Y. Tang, and P. K. Chu, J. Appl. Phys. **84**, 1859 (1998).